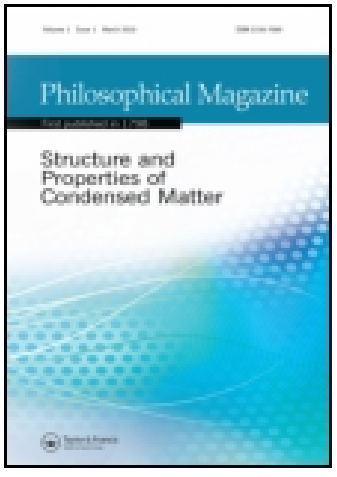

Philosophical Magazine
Publication details, including instructions for authors and subscription information:
http://www.tandfonline.com/loi/tphm20

A simple model to predict long-range atomic ordering temperatures in Cu-based shape memory alloys

J.L. Pelegrina[ab]
[a] División Física de Metales, Centro Atómico Bariloche, Av. E. Bustillo 9500, R8402AGP San Carlos de Bariloche, Argentina
[b] CONICET, Instituto Balseiro, CNEA and Univ. Nac. de Cuyo, Argentina
Published online: 18 Jun 2014.

To cite this article: J.L. Pelegrina (2014) A simple model to predict long-range atomic ordering temperatures in Cu-based shape memory alloys, Philosophical Magazine, 94:24, 2705-2723, DOI: 10.1080/14786435.2014.927600

To link to this article: http://dx.doi.org/10.1080/14786435.2014.927600

Philosophical Magazine, 2014
Vol. 94, No. 24, 2705–2723, http://dx.doi.org/10.1080/14786435.2014.927600

A simple model to predict long-range atomic ordering temperatures in Cu-based shape memory alloys

J.L. Pelegrina*

[a]*División Física de Metales, Centro Atómico Bariloche, Av. E. Bustillo 9500, R8402AGP San Carlos de Bariloche, Argentina;* [b]*CONICET, Instituto Balseiro, CNEA and Univ. Nac. de Cuyo, Argentina*

(*Received 3 February 2014; accepted 19 May 2014*)

The order–disorder and order–order phase transition temperatures in the austenitic phase of Cu-based shape memory alloys were used to obtain a set of first- and second-neighbour pair interchange energies. To this end, a mean field model was postulated. Then, the applicability to different alloys of this simple model was analysed. It was found that a good agreement with the experimental phase diagram is obtained for Cu–Zn–Al, Cu–Al–Ni and Cu–Al–Be alloys using composition-independent parameters. It was also found that for Cu–Al–Mn alloys, composition-dependent pair interchange energies need to be employed.

Keywords: shape memory alloys; copper alloys; order; simulation

1. Introduction

Long-range atomic ordering occurs to the β phase of Cu-based shape memory alloys. Hence, the structure increases its stability and reduces the tendency to decompose into α and γ equilibrium phases at lower temperatures. This β phase presents the martensitic transformation, responsible for the shape-memory behaviour. It has been observed that the martensitic transition temperatures are strongly influenced by the degree of atomic order in Cu–Zn–Al alloys [1]. Therefore, it is important to be aware of the critical temperatures at which ordering is established, because if the ordering temperatures are sufficiently high, the possibility of retaining some degree of disorder through thermal treatments will be reduced and the martensitic transition will be more reproducible.

The high-temperature β phase in Cu-based alloys has a body-centred cubic structure (bcc) with atoms randomly located. After ordering, the atom configurations are best described by taking a cube of $2 \times 2 \times 2$ high temperature bcc cells and defining four interpenetrating face-centred cubic (fcc) sublattices α, β, γ and δ, as shown in Figure 1. It can be seen that each fcc sublattice has a cell parameter twice the size of the one of the bcc structure. Then, each state of order can be defined by assigning the occupation probabilities $P_i^{sublattice}$ of each element i in each sublattice. The most common configurations in Cu-based alloys are characterized by:

*Email: jlp201@cab.cnea.gov.ar

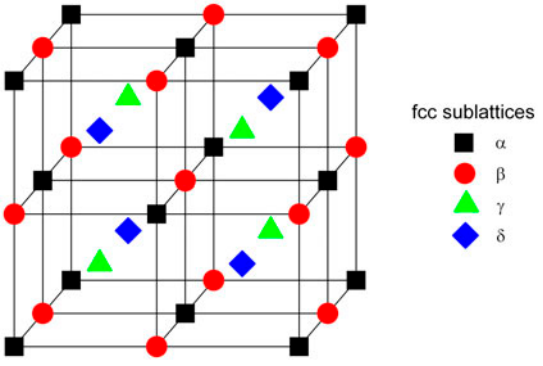

Figure 1. (colour online) Eight bcc cells forming a cube in which four fcc sublattices are defined to describe the ordered structures.

- $P_i^{\alpha} = P_i^{\beta} = P_i^{\gamma} = P_i^{\delta}$ for the disordered A2 (*Im3m*) β phase,
- $P_i^{\alpha} = P_i^{\beta} \neq P_i^{\gamma} = P_i^{\delta}$ for the nearest- (first-) neighbour ordered B2 (*Pm3m*) β_2 phase,
- $P_i^{\alpha} = P_i^{\beta} = P_i^{\gamma} \neq P_i^{\delta}$ for the nearest- and next-nearest-(second-) neighbour ordered DO_3 (*Fm3m*) β_1 phase, and
- $P_i^{\alpha} = P_i^{\beta} \neq P_i^{\gamma} \neq P_i^{\delta} \neq P_i^{\alpha}$ for the nearest- and next-nearest-(second-) neighbour ordered $L2_1$ (*Fm3m*) β_3 phase.

The conditions that must fulfil these occupation probabilities are

$$\sum_i P_i^{sublattice} = 1$$

and

$$P_i^{\alpha} + P_i^{\beta} + P_i^{\gamma} + P_i^{\delta} = 4C_i \tag{1}$$

being C_i the atom concentration of the corresponding element i. These occupation probabilities define the number of atoms of each element in each sublattice. Additionally, it is assumed that the elements within each sublattice are randomly distributed. The different order configurations considered in the current paper and their occupation probabilities are presented in Appendix 1. They constitute alternative atom distributions to the four previously mentioned cases.

It is desirable to obtain the measured ordering temperatures from the corresponding atom configurations. With this purpose, several models (analytical or numerical) with varying degrees of approximation were developed. In most cases, these methods define pair interchange energies, whose values indicate the tendency of a pair of atoms to either order or segregate at a specific distance in the lattice. Being $V_{AB}^{(i)}$ the pairwise interaction energy between A and B atoms at ith neighbouring distance, their pair interchange energy is defined as $W_{AB}^{(i)} = V_{AA}^{(i)} + V_{BB}^{(i)} - 2V_{AB}^{(i)}$. It can be seen that it has a positive value when ordering is favourable. The $W_{AB}^{(i)}$ depend on the pair distance, the

composition, the atomic volume and the temperature [2]. However, only the distance is usually taken into account. This can often be seen in the literature when the $W_{AB}^{(i)}$ estimated from data for the binary alloy are applied to ternary alloys containing A and B atoms. This assumption is a matter of convenience, since it helps to reduce the set of unknowns in the equations. It has also been noticed that in order to calculate critical ordering temperatures, it is enough to consider first- and second-neighbour contributions only. In this way, the $W_{AB}^{(i)}$ can be considered as effective values which take into account the contribution of the interaction with more distant atoms [2].

The aim of the present work is to obtain the pair interchange energies for different Cu-based shape memory alloys from the experimental data in the literature. The analysis will be done by applying the same thermodynamic model and criterion to two binary and four ternary alloys. This will allow to detect the conditions under which the application of the model is valid. It will also be used to observe the behaviour of the $W_{AB}^{(i)}$ with the alloy family (which is not usually taken into account).

The comparison between the experimental data and the simulation will be presented in graphs as a function of either the concentration of a specific element or the electron concentration e/a. The latter variable is the average number of conduction electrons per atom. For the calculation, it was assumed that each Cu or Mn atom contributes with one electron per atom; each Zn or Be with two; each Al with three; and each Ni with 0.6 [3].

2. Theory

The stability of atom distributions in the cubic structure, with and without order, will be predicted from the calculation of the corresponding Gibbs free energies G. To this end, the enthalpy H and entropy S expressions need to be obtained. In the following subsections, the letter A stands for Cu, and letters B and C will be used to indicate generic elements and should not be confused with boron or carbon.

2.1. *Enthalpy expression*

The contribution to the enthalpy that depends on the configuration will be expressed as a sum of the interactions between neighbours. Let $N_{AB}^{(i)}$ be the number of A and B atom pairs at an ith neighbouring distance. Then the term

$$\Sigma^{(i)} = N_{AA}^{(i)}V_{AA}^{(i)} + N_{AB}^{(i)}V_{AB}^{(i)} + N_{AC}^{(i)}V_{AC}^{(i)} + N_{BB}^{(i)}V_{BB}^{(i)} + N_{BC}^{(i)}V_{BC}^{(i)} + N_{CC}^{(i)}V_{CC}^{(i)} \tag{2}$$

represents the contribution to the enthalpy of a distribution of atoms in ith neighbouring positions in a ternary alloy. By introducing the concept of pair interchange energies $W_{AB}^{(i)} = V_{AA}^{(i)} + V_{BB}^{(i)} - 2V_{AB}^{(i)}$, Equation (2) can be rewritten as the sum of two terms. One of them is called $\Sigma_{amount}^{(i)}$ as it depends on the amount of atoms and not on their configuration. It is expressed as

$$\Sigma_{amount}^{(i)} = Z^{(i)}\left[N_A V_{AA}^{(i)} + N_B V_{BB}^{(i)} + N_C V_{CC}^{(i)}\right]$$

being $Z^{(i)}$ the number of ith neighbours and N_A, N_B and N_C the number of A, B and C atoms, respectively, in the volume under consideration. The other term is called $\Sigma^{(i)}_{configuration}$ as it depends on the particular configuration that the atoms adopt in the solid. It is expressed as

$$\Sigma^{(i)}_{configuration} = -\left[N^{(i)}_{AB}W^{(i)}_{AB} + N^{(i)}_{AC}W^{(i)}_{AC} + N^{(i)}_{BC}W^{(i)}_{BC}\right] \Big/ 2$$

When analysing atomic ordering, as the number of pairs is altered, the latter term will reflect the energy change which occurs during the transition. In order to obtain the enthalpy contribution, it is necessary to divide this expression by the total number of atoms, $N = N_A + N_B + N_C$. As usually, only first- and second-neighbours will be taken into account, and the term to be evaluated is, therefore, given by

$$H/N = -\left[N^{(1)}_{AB}W^{(1)}_{AB} + N^{(1)}_{AC}W^{(1)}_{AC} + N^{(1)}_{BC}W^{(1)}_{BC} + N^{(2)}_{AB}W^{(2)}_{AB} + N^{(2)}_{AC}W^{(2)}_{AC} + N^{(2)}_{BC}W^{(2)}_{BC}\right] \Big/ 2N \tag{3}$$

2.2. *Entropy expression*

The configurational entropy of each atom distribution was calculated using an irregular tetrahedron as the basic cluster, following the cluster variation method in the bcc lattice [4–6]. It is given by

$$\begin{aligned} S/(k_{\mathrm{B}}N) = -\Bigg\{ & 6\sum_{ijkl} L\left(Z^{\alpha\beta\gamma\delta}_{ijkl}\right) - 3\sum_{ijk}\left[L\left(U^{\alpha\beta\gamma}_{ijk}\right) + L\left(U^{\alpha\beta\delta}_{ijk}\right) + L\left(U^{\alpha\gamma\delta}_{ijk}\right) + L\left(U^{\beta\gamma\delta}_{ijk}\right)\right] \\ & + 3\sum_{ij}\left[L\left(R^{\alpha\beta}_{ij}\right) + L\left(R^{\gamma\delta}_{ij}\right)\right]/2 + \sum_{ij}\left[L\left(Y^{\alpha\gamma}_{ij}\right) + L\left(Y^{\alpha\delta}_{ij}\right) + L\left(Y^{\beta\gamma}_{ij}\right) + L\left(Y^{\beta\delta}_{ij}\right)\right] \\ & - \sum_{i}[L\left(X^{\alpha}_{i}\right) + L\left(X^{\beta}_{i}\right) + L(X^{\gamma}_{i}) + L\left(X^{\delta}_{i}\right)]/4 \Bigg\} \end{aligned} \tag{4}$$

where k_{B} is the Boltzmann's constant, the sums are over the atomic species, the Greek supraindices stand for the different sublattices and $L(x) = x\ln(x)$. The basic variables of the treatment are the probabilities $Z^{\alpha\beta\gamma\delta}_{ijkl}$ that a tetrahedron adopts a configuration of i, j, k and l atoms on α, β, γ and δ sublattice positions. The subclusters are the triangle, represented by the U_{ijk}, the second-neighbour pair (R_{ij}), the first-neighbour pair (Y_{ij}) and the point probability (X_i). These latter variables are derived as linear combinations of the tetrahedron probabilities by the following reduction relations

$$\begin{aligned} U^{\alpha\beta\gamma}_{ijk} &= \sum_{l} Z^{\alpha\beta\gamma\delta}_{ijkl} \\ R^{\alpha\beta}_{ij} &= \sum_{kl} Z^{\alpha\beta\gamma\delta}_{ijkl} \\ Y^{\alpha\gamma}_{ik} &= \sum_{jl} Z^{\alpha\beta\gamma\delta}_{ijkl} \\ X^{\alpha}_{i} &= \sum_{jkl} Z^{\alpha\beta\gamma\delta}_{ijkl} \end{aligned} \tag{5}$$

and, correspondingly, for the other sublattice combinations. As an equation for controlling the calculation of the tetrahedron probabilities, the equality $P_i^{sublattice} = X_i^{sublattice}$ ought to be taken into account.

2.3. *Strategy for phase stability evaluation*

A computer programme was used to create the distributions for the different atomic orders and to evaluate their enthalpy and entropy differences. To this end, a cube of $120 \times 120 \times 120$ unit bcc cells (A2 order) was defined and the four sublattices α, β, γ and δ were introduced. This cube, which contains 3.456×10^6 atoms, has proved to be big enough to avoid the appearance of features due to improper statistics [7]. The different atom species were distributed on these sublattice sites in such a way that either the completely disordered state or the perfect long-range order (as imposed by the occupation probabilities presented in Appendix 1) was obtained. Within each sublattice the elements were randomly arranged. The programme then counted the number of first- and second-neighbour pairs which were used for the calculation of Equation (3). The tetrahedron probabilities were also assessed and the variables in Equation (5) were obtained for the evaluation of Equation (4). Periodic conditions were applied at the borders of the cube. In this way, the contribution to the free energy due to the atom configuration ($G = H - TS$) and the relative stability for each temperature T could be obtained. It is customary to work with Equations (3) and (4) since this makes the calculation independent of the number of atoms. Therefore, Equation (3) is divided by k_B and the pair interchange energies are expressed in Kelvin units.

From the measured ordering temperatures (T_M), the pair interchange energies were guessed. To this end, the critical temperatures (T_C) were calculated by matching the free energies of the corresponding configurations. For instance, if configurations 1 and 2 are considered, the critical temperature is given by

$$T_C = \frac{H(\text{configuration 2}) - H(\text{configuration 1})}{S(\text{configuration 2}) - S(\text{configuration 1})}$$

The strategy was to minimize the difference between T_M and T_C, and control that no other atom configuration had a lower energy value in the whole temperature range of each phase field. This is of great importance since there are different sets of pair interchange energies that are more efficient to predict the critical ordering temperatures, but they favour the appearance of atom configurations that are in disagreement with those reported in the literature. Hence, all atom configurations presented in Appendix 1 were considered when comparing the free energies to reject specific values of the pair interchange energies. This strategy was applied not to a single composition/order transition, but to the whole set of available experimental data. This means that the minimization was conducted on a certain composition range and took into account one or two ordering transitions, depending on the alloy system. The pair interchange energies were taken from the fit that better reduced the differences between T_M and T_C for all the available data.

It has to be noted that in the present calculations, the possibility of short-range order and of a continuous character in the long-range order transitions have been excluded. These simplifications allow an easier implementation of the model. Then, it should be considered that the model does not reproduce the real distribution of atoms but, as shown next, will permit a proper prediction of the critical ordering temperatures.

3. First- and second-neighbour pair interchange energies

3.1. *Cu–Zn*

This system presents one ordering transition from the high-temperature A2 phase to the low-temperature B2 phase in near equiatomic concentrations. The experimental critical temperatures [8–14] are quite insensitive to the composition variations, as shown in Figure 2. This ordinate axis range will be used throughout the different cases and will serve for a better comparison of the quality of the calculations.

The application of the evaluation strategy shows that several pairs of first- and second-neighbour interchange energies provide a good fit of the data. These sets are linearly related, as shown in Figure 3, by the equation

$$W^{(2)}_{\mathrm{CuZn}} = 1.323\, W^{(1)}_{\mathrm{CuZn}} - 642\,\mathrm{K} \tag{6}$$

When different energy values are taken, the calculated critical ordering temperatures fall between the lower black line and the upper red line shown in Figure 2. This small variation hinders the determination of a single set of interchange energies as the best fit to the experimental data. The condition $W^{(1)}_{\mathrm{CuZn}} < 960\,\mathrm{K}$ is a constrain to avoid the appearance of the DO_3 phase in the B2 phase field. Apparently, there is no lower limit to the first-neighbour interchange energy and even negative values are permitted. This apparent contradiction, that a negative value would tend to disorder the first-neighbour pairs, is counteracted by an even higher tendency to disorder Cu–Zn pairs at second-neighbour distances.

The pair interchange energies proposed by Inden [15], $W^{(1)}_{\mathrm{CuZn}} = 955\,\mathrm{K}$ and $W^{(2)}_{\mathrm{CuZn}} = 535\,\mathrm{K}$, were assumed as reliable values by many authors, independently of the model applied to perform calculations. In the present scheme, these interchange energies do not fit the experimental values properly, predicting critical ordering temperatures overestimated in around 12%. It can be seen in Figure 3 that the energies proposed by Inden fall out of the linear relation established in the present work.

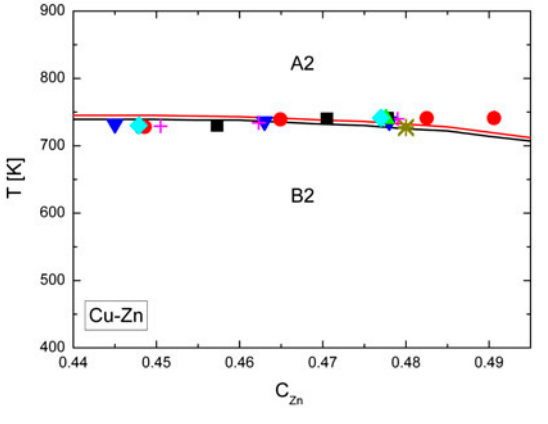

Figure 2. (colour online) Critical ordering temperatures as a function of composition in Cu–Zn alloys taken from: [8] squares, [9] circles, [10] up triangle, [11] down triangles, [12] diamonds, [13] plus signs and [14] asterisks. The full lines join calculated values, see text for details.

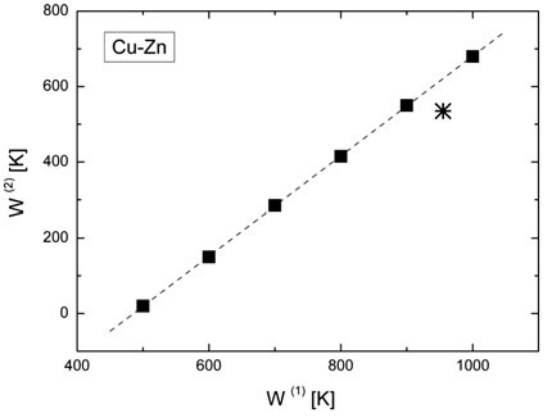

Figure 3. Pairs of first- and second-neighbour interchange energies that optimize the fit of the experimental data (squares). The line shows the linear behaviour of these points. The asterisk corresponds to the energies proposed by Inden [15].

3.2. *Cu–Al*

This system presents the A2 phase at high temperatures and it becomes ordered by lowering the temperature to DO_3 or $L2_1$ when the Al concentration is below or above 0.25, respectively. There is a slight variation of the experimental critical temperatures with composition [14,16–18], as shown in Figure 4.

In the present alloy system, the presence of two ordered structures at low temperatures enables the unique determination of the pair interchange energies

$$W^{(1)}_{\mathrm{CuAl}} = 1010\,\mathrm{K} \quad W^{(2)}_{\mathrm{CuAl}} = 1070\,\mathrm{K}$$

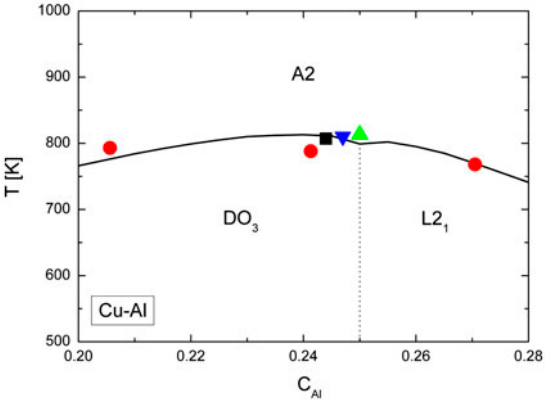

Figure 4. (colour online) Critical ordering temperatures as a function of composition in Cu–Al alloys taken from: [14] square, [16] circles, [17] up triangle and [18] down triangle. The full line join calculated values.

The black line in Figure 4 was drawn calculating ordering temperatures with these energy values. It can be seen that the curve fits the experimental data well.

3.3. *Cu–Zn–Al*

There is plenty of experimental information on the β phase of this ternary alloy system. For a constant electron concentration of 1.48, the different ordered phases can be presented as a function of C_{Zn} (see Figure 5). Similarly to the Cu–Al case, this system presents the A2 phase at high temperature and orders on lowering the temperature to DO_3 for compositions with Zn content up to 0.05 [14]. Between 0.05 and 0.11, there seems to be only one ordering reaction from A2 to $L2_1$ (see Figure 5 and [14]). Finally, for higher Zn concentrations up to 0.28, two ordering transitions occur. The first one varies from A2 to B2 and, on further cooling, B2 is changed to $L2_1$ order. The ordering transition temperatures departing from the A2 phase do not seem to depend strongly on composition. On the other hand, the B2 to $L2_1$ transitions vary within a wide range of temperatures depending on the Zn concentration. For higher concentrations, the B2 to $L2_1$ transition temperature is too low, and reliable measurements are not available.

The critical temperatures were fitted using the conventional atom configurations for Cu–Zn–Al. They are listed in Appendix 1 as: section B for A2, sections D and D1 for B2 and sections H and H1 for $L2_1$. Six interchange energies are involved in this ternary alloy. It is not possible to make a good fit using the Cu–Al values presented in the previous section and adjusting the other four parameters, with the condition imposed by Equation (6). Instead, the minimization procedure has to be performed by varying the six energy values. The appearance of undesired order configurations at the different temperatures needs to be carefully monitored. The best fit is obtained with

$$W^{(1)}_{\mathrm{CuZn}} = 850\,\mathrm{K} \quad W^{(2)}_{\mathrm{CuZn}} = 485\,\mathrm{K}$$

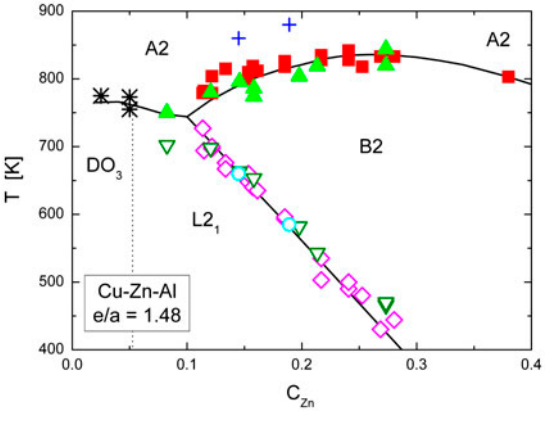

Figure 5. (colour online) Critical ordering temperatures as a function of Zn concentration in Cu–Zn–Al alloys at constant electron concentration ($e/a = 1.48$) taken from: [14] asterisks, squares and diamonds, [19] up and down triangles, [20] plus signs and circles. The full lines join calculated values.

$$W^{(1)}_{\mathrm{CuAl}} = 1150\,\mathrm{K} \quad W^{(2)}_{\mathrm{CuAl}} = 860\,\mathrm{K}$$

$$W^{(1)}_{\mathrm{AlZn}} = -100\,\mathrm{K} \quad W^{(2)}_{\mathrm{AlZn}} = 400\,\mathrm{K}$$

These energy values allowed to draw the full lines in Figure 5, showing that the simulation agrees quite well with the measured values within experimental scatter. The dotted line separating the DO_3 from the $L2_1$ phase fields was drawn for the composition at which the $L2_1$ ordering temperature exceeds that of DO_3 by more than 2 K, twice the scatter of the simulation runs.

The pair interchange energies obtained for Cu–Zn–Al can be compared with those taken from the literature and presented in Table 1. In the first two cases ([14] and [19]), the Cu–Zn pair energies were taken from Inden [15], assuming their independence of composition. The main difference in the Cu–Al nearest-neighbour energy values between [14] and [19] must be ascribed to the mathematical model used for the fit. In [14] Monte Carlo simulations were performed within the Blume–Emery–Griffiths model, whereas in [19] the Bragg–Williams–Gorski approximation (BWGA) was used. On the other hand, the third case in Table 1 shows what happens when the Al–Zn energies are neglected, based on the absence of intermetallic phases in the phase diagram. As the pair interchange energies are effective values which include the contributions of neighbours that are not specifically taken into account, the imposition of zero to some of the $W^{(i)}_{\mathrm{AB}}$ has an important effect in the value of the others. Therefore, it is advisable not to impose these restrictions beforehand, and only expect to obtain small values for these Al–Zn pair energies. The satisfactory results encourage the analysis of other ternary alloys.

Table 1. Pair interchange energies in Cu–Zn–Al from the literature.

Reference	$W^{(1)}_{\mathrm{CuAl}}$ [K]	$W^{(2)}_{\mathrm{CuAl}}$ [K]	$W^{(1)}_{\mathrm{CuZn}}$ [K]	$W^{(2)}_{\mathrm{CuZn}}$ [K]	$W^{(1)}_{\mathrm{AlZn}}$ [K]	$W^{(2)}_{\mathrm{AlZn}}$ [K]
[14]	1660	920	955	535	−45	285
[19]	1345	825	955	535	−50	200
[20]	905	130	545	95	0	0

3.4. *Cu–Al–Ni*

This alloy system presents two ordering transitions: A2–B2 and B2–$L2_1$, where A2 is the disordered high-temperature phase and $L2_1$ is the ordered low-temperature phase. It is not possible to present the data as in Cu–Zn–Al, since the data from the literature do not correspond to a constant electron concentration. Therefore, the critical temperatures are shown for fixed concentrations of one of the elements (see Figure 6).

The ordered atom configurations in the present case are assumed to be different from those for Cu–Zn–Al. Taking into account the high affinity between Ni and Al, and following the suggestion by [20,21], Ni was always placed as a nearest neighbour of Al in the ordered structures. The configurations used are listed in Appendix 1 as: B for A2, D and D3 for B2 and H and H3 for $L2_1$. Following a similar fitting procedure, the best result was obtained with

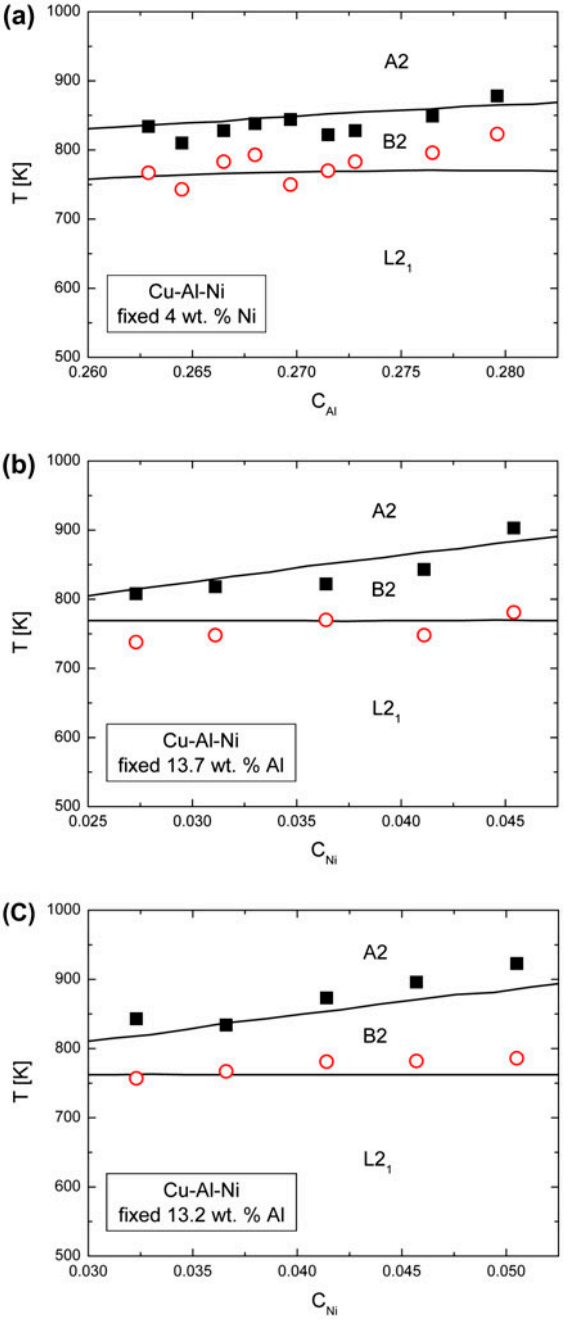

Figure 6. (colour online) Critical ordering temperatures in Cu–Al–Ni alloys taken from [21]. (a) Fixed Ni content at 4 wt. %, (b) fixed Al content at 13.7 wt. % and (c) fixed Al content at 13.2 wt. %. The full lines join calculated values.

$$W^{(1)}_{\mathrm{CuAl}} = 1080\,\mathrm{K} \quad W^{(2)}_{\mathrm{CuAl}} = 670\,\mathrm{K}$$

$$W^{(1)}_{\mathrm{CuNi}} = -40\,\mathrm{K} \quad W^{(2)}_{\mathrm{CuNi}} = 80\,\mathrm{K}$$

$$W^{(1)}_{\mathrm{AlNi}} = 1460\,\mathrm{K} \quad W^{(2)}_{\mathrm{AlNi}} = -350\,\mathrm{K}$$

These energy values allowed to draw the full lines in Figure 6. Again, the simulation agrees reasonably well with the measured values within experimental scatter. It is interesting to note that, as in the Al–Zn case, the first-neighbour pair interchange energy for Cu–Ni is negative and has an absolute value smaller than the second-neighbour term. This similarity can be rationalized by noting that there are no long-range ordered phases in the corresponding binary diagrams ([22]: page 239 for Al–Zn and page 1442 for Cu-Ni).

In [21], the Cu–Al–Ni pair interchange energies were used, taking Cu–Al values from [19], Al–Ni from [23] and imposing Cu–Ni to zero, based on the absence of long-range order in the binary phase diagram. The proposed energies were $W^{(1)}_{\mathrm{CuAl}} = 1345\,\mathrm{K}$, $W^{(2)}_{\mathrm{CuAl}} = 825\,\mathrm{K}$, $W^{(1)}_{\mathrm{CuNi}} = 0\,\mathrm{K}$, $W^{(2)}_{\mathrm{CuNi}} = 0\,\mathrm{K}$, $W^{(1)}_{\mathrm{AlNi}} = 3080\,\mathrm{K}$ and $W^{(2)}_{\mathrm{AlNi}} = 1880\,\mathrm{K}$. It was also necessary to define a net chemical interchange energy at nearest-neighbour positions to reproduce the observed critical temperatures [21]. A comparison with Figure 3 in [21] indicates that this feature improves the simulation. However, in the present work this concept was disregarded, since it was considered an unnecessary complication of the model. It was also found that it is not wise to set to zero the Cu–Ni energies in Equation (3), because these values stabilize improper atom configurations.

It is expected that the pair interchange energies obtained for a binary alloy should remain valid for low contents of the third element in a ternary alloy. It can be seen that for Cu–Al pairs (in alloys with Ni compositions from 0.03 to 0.05) the first-neighbour interchange energy had to be increased by around 7%, whereas the second-neighbour term had to be decreased by about 37% with respect to the binary alloy values. This implies that the apparent low Ni content is, however, sufficiently high and sets a limit to what can be considered "low contents of the third element". Therefore, it is advisable to confine the use of pair interchange energies strictly to compositions within the range used for their determination.

3.5. *Cu–Al–Be*

In spite of all the research done in recent years, there are few studies of ordering for this system [18,24,25]. The available data belong to alloys with $0.2219 \le C_{\mathrm{Al}} \le 0.2313$, i.e. a small composition variation and, therefore, Figure 7 shows the data as a function of Be concentration. The alloys present only one transition from the disordered high-temperature A2 phase. The ordered low-temperature phase has been proposed as DO_3, based on X-ray diffraction measurements in powdered specimens [24] where the experimental results were compared with theoretical estimations and the ratio of the intensities of two room temperature superlattice reflections peaks was calculated. As the intensity of diffraction peaks can be easily perturbed by experimental conditions (for example: a small amount of texture), some doubts about the determination of the stable ordered configuration by this method might arise. Another way to address the problem is by

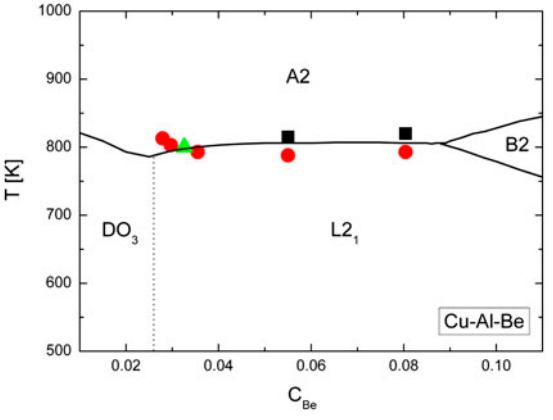

Figure 7. (colour online) Critical ordering temperatures as a function of Be concentration in Cu–Al–Be alloys taken from: [18] squares, [24] circles, [25] triangle. The full line join calculated values for fixed 22.7 at. % Al.

comparison with the Cu–Zn–Al alloys and its binary constituents. The Cu–Zn and Cu-Be alloys present ordering for equiatomic compositions, whereas Al–Zn and Al–Be are free of ordered phases in the whole composition range ([22]: pages 1508, 644, 239 and 125, respectively). Then, it is tempting to expect similar ordering reactions for composition ranges delimited by the number of non-Cu atoms, as a first approximation. Figure 5 shows that a single transition from A2 to $L2_1$ happens for $0.052 \leq C_{Zn} \leq 0.100$ and $e/a = 1.48$. This is equivalent to a non-Cu atoms composition interval of $0.266 \leq C_{Zn} + C_{Al} \leq 0.290$. On the other hand, the experimental data in Figure 7 have compositions in the interval $0.259 \leq C_{Al} + C_{Be} \leq 0.302$. Hence, a similar behaviour is expected and, therefore, if the number of non-Cu atoms exceeds the occupation capacity of sublattice δ, the $L2_1$ type configuration is adopted. The excess non-Cu atoms will only go to sublattice γ.

The critical temperatures were fitted using similar atom configurations as for Cu–Zn–Al. They are listed in Appendix 1 as: B for A2 and H and H1 for $L2_1$. Following a similar fitting procedure, the best result was obtained with

$$W^{(1)}_{CuAl} = 1210\,K \quad W^{(2)}_{CuAl} = 900\,K$$

$$W^{(1)}_{CuBe} = 635\,K \quad W^{(2)}_{CuBe} = 125\,K$$

$$W^{(1)}_{AlBe} = -85\,K \quad W^{(2)}_{AlBe} = 330\,K$$

These energy values allowed to draw the full lines in Figure 7, taking a mean Al concentration of 0.227, showing that the simulation agrees reasonably well with the measured values within experimental scatter. The dotted line separating the DO_3 from the $L2_1$ phase fields was drawn for the composition at which the $L2_1$ ordering temperature exceeds that of DO_3 by more than 2 K, twice the scatter of the simulation runs. It can also be seen that the B2 phase is expected for Be concentrations larger than 0.089.

In [24], the Cu–Al–Be pair interchange energies were fitted using a mean field model, which is essentially based on the BWGA. The result was $W^{(1)}_{\mathrm{CuAl}} = 1149\,\mathrm{K}$, $W^{(2)}_{\mathrm{CuAl}} = 766\,\mathrm{K}$, $W^{(1)}_{\mathrm{CuBe}} = 2747\,\mathrm{K}$, $W^{(2)}_{\mathrm{CuBe}} = 1831\,\mathrm{K}$, $W^{(1)}_{\mathrm{AlBe}} = 3347\,\mathrm{K}$ and $W^{(2)}_{\mathrm{AlBe}} = 2231\,\mathrm{K}$. The authors claim that the narrow range of the measured critical temperatures only makes the Cu–Al values trustworthy. They recognize that the positive Al–Be energies imply an ordering tendency which is opposite to the segregation that is known to occur. Notwithstanding, they use these values within the concept of effective coefficients, allowing to reproduce the observed ordering transitions.

As in the Al–Zn and Cu–Ni cases, the first-neighbour pair interchange energy for Al–Be is negative and has an absolute value smaller than the second-neighbour term. Again, this can be related to the fact that there are no long-range ordered phases in the binary Al–Be diagram ([22]: page 125). Instead, when the first-neighbour pair interchange energy obtained in the ternary alloys is positive and has a value higher than the second-neighbour term, order is expected in the binary phase diagram. This holds for Cu–Al, Cu–Zn, Al–Ni and Cu–Be. It could be further argued that the negative second-neighbour term in Al–Ni emphasizes the B2 ordering tendency, being responsible for the absence of an A2 structure in this binary alloy.

3.6. *Cu–Al–Mn*

As in Cu–Al–Ni, the two ordering transitions change the disordered A2 phase to B2 at high temperatures, and then B2 to $L2_1$. There is a wide composition range for which the ordering temperatures were reported for this family of alloys [17,26–28]. The ranges are $0.18 \le C_{\mathrm{Al}} \le 0.30$, $0.01 \le C_{\mathrm{Mn}} \le 0.25$, maintaining the electron concentration within $1.375 \le e/a \le 1.750$. The critical temperatures have to be presented for fixed concentrations of one of the elements. Otherwise, a cloud of experimental points in the graphs is obtained. Some examples are shown in Figure 8 for fixed Mn (a, b and c) or Al (d) concentrations.

The critical temperatures were fitted using similar atom configurations as for Cu–Zn–Al. They are listed in Appendix 1 as: B for A2, D and D1 for B2, and H and H1 for $L2_1$. Calculations reveal that it is not feasible to maintain the hypothesis of composition-independent $W^{(i)}_{AB}$. Even for 20 at. % Mn, it is not possible to obtain energies that allow the proper simulation of the whole Al range, as shown in Figure 8(a). Instead, a good fit is achieved only after limiting the Al concentration below 0.26. The pair interchange energies obtained are listed in Table 2. Following a similar fitting procedure for 15 at. % Mn, limiting the Al concentration below 0.26, a reasonable agreement can be found between experiments and simulations. This is shown in Figure 8(b), with the corresponding parameters listed in Table 2.

The observed variation of the pair interchange energies with Mn concentration induces to examine the possibility of a linear relationship between the $W^{(i)}_{AB}$ and C_{Mn}. To this end, the pair interchange energies for 15 at. % Mn and 20 at. % Mn were linearly extrapolated to 10 at. % Mn, as presented in Table 2. Figure 8(c) shows the experimental results and the simulated lines for both transitions: A2 to B2 (dotted line) and B2 to $L2_1$ (dashed line). It can be seen that the latter transition is properly predicted whereas the former is far from being adequate. The good set of fitted parameters stands also in Table 2, from which the full lines in Figure 8(c) were obtained. It shows

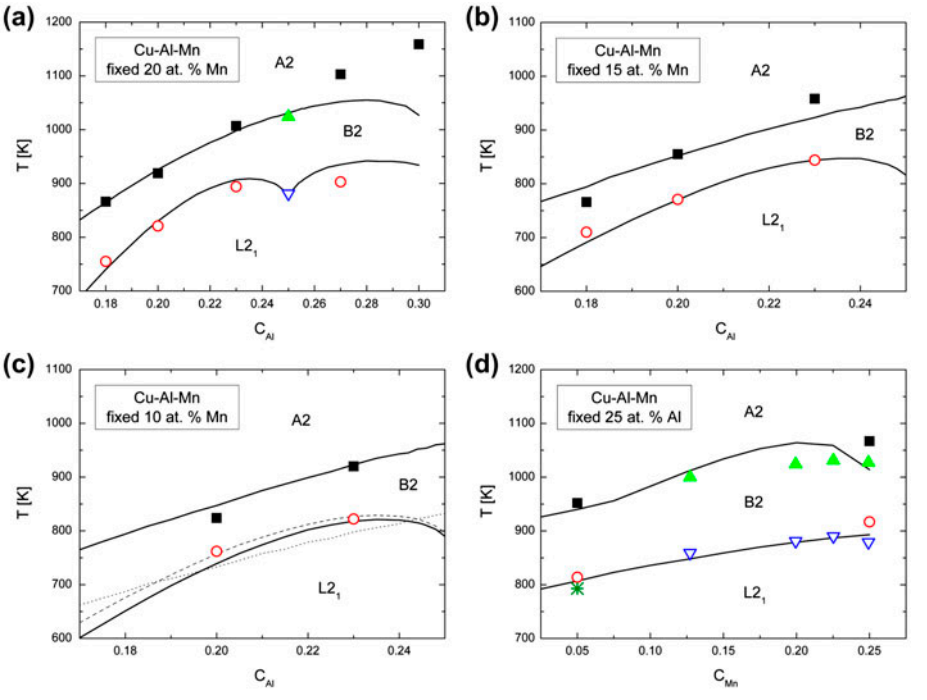

Figure 8. (colour online) Critical ordering temperatures in Cu–Al–Mn alloys taken from: [27] squares and circles, [17] up and down triangles, [28] asterisk. (a) Fixed Mn content at 20 at. %, (b) fixed Mn content at 15 at. %, (c) fixed Mn content at 10 at. % and (d) fixed Al content at 25 at. % Al. The full lines join calculated values with the best fitting parameters. The dotted and dashed lines in (c) correspond to the simulation with the extrapolated values presented in Table 2.

Table 2. Pair interchange energies for Cu–Al–Mn when one of the elements is at a fixed concentration. See text for details.

Element fixed	$W^{(1)}_{CuAl}$ [K]	$W^{(2)}_{CuAl}$ [K]	$W^{(1)}_{CuMn}$ [K]	$W^{(2)}_{CuMn}$ [K]	$W^{(1)}_{AlMn}$ [K]	$W^{(2)}_{AlMn}$ [K]
20 at. % Mn	1600	900	−30	200	−360	830
15 at. % Mn	1450	890	30	250	−330	770
10 at. % Mn extrapolated values	1300	880	90	300	−300	710
10 at. % Mn adjusted values	1400	860	90	240	−300	690
25 at. % Al	1350	720	1040	−50	1570	830

that the linear extrapolation underestimated the value of $W^{(1)}_{AlCu}$. This leads to conclude that the pair interchange energies do not have a simple and predictable composition dependence in the case of Cu–Al–Mn.

In Figure 8(d), the transition temperatures for fixed 25 at. % Al, together with the delimiting lines obtained from the simulation (using the parameters shown in Table 2)

are presented. The prediction is accurate, despite the bad looking points for the A2 to B2 transition at high Mn content (because the spread is not higher than 40 K, well within the scatter of the experiments). The most surprising feature arises from the comparison of the pair interchange energies in Table 2. Again, it seems not possible to fit the data for fixed Al content with values next to those for fixed Mn content. In particular, $W^{(1)}_{\mathrm{CuMn}}$ and $W^{(1)}_{\mathrm{AlMn}}$ need to take positive values above 1000 K for the dual purpose of obtaining a good fit and avoiding undesired order configurations (when the Al composition is not changed).

In [26], the Cu–Al–Mn pair interchange energies were fitted as $W^{(1)}_{\mathrm{CuAl}} = 1605\,\mathrm{K}$, $W^{(2)}_{\mathrm{CuAl}} = 856\,\mathrm{K}$, $W^{(1)}_{\mathrm{CuMn}} = 1266\,\mathrm{K}$, $W^{(2)}_{\mathrm{CuMn}} = 353\,\mathrm{K}$, $W^{(1)}_{\mathrm{AlMn}} = 2144\,\mathrm{K}$ and $W^{(2)}_{\mathrm{AlMn}} = 1168\,\mathrm{K}$ using the BWGA, and adjusting own experimental values and those extracted from [17]. The latter data belong all to 25 at. % Al, while the former fall in the range from 18.7 to 24.4 at. % Al. The increased values of the fitted pair interchange energies could be ascribed to the mix of compositions. However, this hypothesis deserves more analysis.

Finally, it can be said that the critical ordering temperatures can be predicted in limited composition ranges in Cu–Al–Mn. Notwithstanding, this family of alloys presents a behaviour with regard to the pair interchange energies that differs from the other ternary alloys studied in the present work. Therefore, the model should be modified when Mn atoms are considered in the alloy.

4. Conclusions

Long-range order in Cu-based shape memory alloys has been analysed in terms of a Gibbs free energy model. The best set of pair interchange energies was deduced for each alloy using an energy expression which solely takes into account the nearest- and next-nearest-neighbours, and an entropy treatment coming from the cluster variation method. It is concluded that:

- The energies can be determined from the experimental ordering temperatures. To this end, it is important to simultaneously control that, during the fit, the energy values do not favour the appearance of other ordered phases in the known phase fields.
- The pair interchange energies are specific for each alloy. These energies depend on the particular expression used for the energy and the entropy. Therefore, data need to be carefully handled when using pair interchange energies from different sources in the literature.
- The pair interchange energies suitable for ternary alloys differ from those appropriate for binary alloys. For instance, in ternary systems, the pair energies belonging to a binary system (which does not exhibit long-range ordering) should not be set to zero beforehand.
- For the ternary alloys Cu–Zn–Al, Cu–Al–Ni and Cu–Al–Be, the pair interchange energies are independent of composition.
- For Cu–Al–Mn alloys, the pair interchange energies are valid within very limited composition ranges. They also present a complex variation as regards composition.

Acknowledgements

This work was supported by the ANPCyT, CONICET, CNEA and Universidad Nacional de Cuyo, Argentina. Helpful discussions with Drs F. Laguna, F.C. Lovey and M. Sade are gratefully acknowledged. The author wishes to thank Dr P. Arneodo Larochette for a critical reading of the manuscript.

References

[1] R. Rapacioli and M. Ahlers, Acta Metall. 27 (1979) p.777.
[2] M. Ahlers, Mater. Sci. Eng. A 349 (2003) p.120.
[3] T.B. Massalski and H.W. King, Prog. Mater. Sci. 10 (1961) p.1.
[4] R. Kikuchi and C.M. van Baal, Scr. Metall. 8 (1974) p.425.
[5] H. Ackermann, G. Inden and R. Kikuchi, Acta Metall. 37 (1989) p.1.
[6] C. Colinet, G. Inden and R. Kikuchi, Acta Metall. Mater. 41 (1993) p.1109.
[7] M. Ahlers and J.L. Pelegrina, Mater. Sci. Eng. A 356 (2003) p.298.
[8] C. Sykes and H. Wilkinson, J. Inst. Met. 61 (1937) p.223.
[9] D.N. Yoon and A. Bienenstock, Phys. Rev. 170 (1968) p.631.
[10] J. Ashman and P. Handler, Phys. Rev. Lett. 23 (1969) p.642.
[11] R. Crombie and D.B. Downie, Acta Metall. 19 (1971) p.1227.
[12] M.M. Shea and N.S. Stoloff, Metall. Trans. 5 (1974) p.755.
[13] P.K. Kumar and L. Muldawer, Phys. Rev. B 14 (1976) p.1972.
[14] F. Lanzini, R. Romero, M. Stipcich and M.L. Castro, Phys. Rev. B 77 (2008) p.134207/1.
[15] G. Inden, Z. Metallkd. 66 (1975) p.648.
[16] J. Jellison and E.P. Klier, Trans. Metall. Soc. AIME 233 (1965) p.1694.
[17] M. Bouchard and G. Thomas, Acta Metall. 23 (1975) p.1485.
[18] F. Lanzini, R. Romero and M.L. Castro, Intermetallics 16 (2008) p.1090.
[19] R. Rapacioli and M. Ahlers, Scr. Metall. 11 (1977) p.1147.
[20] A. Planes, L. Mañosa, E. Vives, J. Rodríguez-Carvajal, M. Morin, G. Guénin and J.L. Macqueron, J. Phys.: Condens. Matter 4 (1992) p.553.
[21] V. Recarte, O.A. Lambri, R.B. Pérez-Sáez, M.L. Nó and J. San Juan, Appl. Phys. Lett. 70 (1997) p.3513.
[22] T.B. Massalski (ed.-in-chief), H. Okamoto, P.R. Subramanian and L. Kacprzak (eds.), *Binary Alloy Phase Diagrams*, 2nd ed., ASM International, Materials Park, OH, 1990.
[23] M. Ahlers, Philos. Mag. A 70 (1994) p.247.
[24] M. Jurado, T. Castàn, L. Mañosa, A. Planes, J. Bassas, X. Alcobé and M. Morin, Philos. Mag. A 75 (1997) p.1237.
[25] S. Montecinos, A. Cuniberti, M.L. Castro and R. Boeri, J. Alloys Compd. 467 (2009) p.278.
[26] M. Prado, M. Sade and F. Lovey, Scr. Metall. Mater. 28 (1993) p.545.
[27] R. Kainuma, N. Satoh, X.J. Liu, I. Ohnuma and K. Ishida, J. Alloys Compd. 266 (1998) p.191.
[28] E. Obradó, C. Frontera, L. Mañosa and A. Planes, Phys. Rev. B 58 (1998) p.14245.

Appendix 1

In the present section the occupation probabilities for the different atom configurations will be given, with the exception of those for Cu, that can be obtained from Equation (1). All the Cu-based alloys considered in the present work are of the form Cu-*A* in the binary case or Cu-Al-A for the ternary.

- A2 order

- A) Binary alloys

$$P_A^{\alpha} = P_A^{\beta} = P_A^{\gamma} = P_A^{\delta} = C_A$$

- B) Ternary alloys

$$P_{\mathrm{Al}}^{\alpha} = P_{\mathrm{Al}}^{\beta} = P_{\mathrm{Al}}^{\gamma} = P_{\mathrm{Al}}^{\delta} = C_{\mathrm{Al}}$$

$$P_A^{\alpha} = P_A^{\beta} = P_A^{\gamma} = P_A^{\delta} = C_A$$

- B2 order

- C) Binary alloys

$$P_A^{\alpha} = P_A^{\beta} = 0 \qquad P_A^{\gamma} = P_A^{\delta} = 2C_A$$

- D) Ternary alloys

$$P_{\mathrm{Al}}^{\alpha} = P_{\mathrm{Al}}^{\beta} = 0 \qquad P_{\mathrm{Al}}^{\gamma} = P_{\mathrm{Al}}^{\delta} = 2C_{\mathrm{Al}}$$

and with three alternatives for the third element because it can be equally distributed:

- D1) In γ and δ

$$P_A^{\alpha} = P_A^{\beta} = 0 \qquad P_A^{\gamma} = P_A^{\delta} = 2C_A$$

- D2) In α, β, γ and δ

$$P_A^{\alpha} = P_A^{\beta} = P_A^{\gamma} = P_A^{\delta} = C_A$$

- D3) In α and β

$$P_A^{\alpha} = P_A^{\beta} = 2C_A \qquad P_A^{\gamma} = P_A^{\delta} = 0$$

- DO_3 order

- E) Binary alloys with:

- Ea) $C_A \leq 0.25$

$$P_A^{\alpha} = P_A^{\beta} = P_A^{\gamma} = 0 \qquad P_A^{\delta} = 4C_A$$

- Eb) $C_A > 0.25$

$$P_A^{\alpha} = P_A^{\beta} = P_A^{\gamma} = 1 - 4C_{\mathrm{Cu}}\ /3 \qquad P_A^{\delta} = 1$$

- F) Ternary alloys with the third element:
  - F1) In δ and equally distributed in α, β, γ, and:
    - F1a) $C_{Al} \leq 0.25$

$$P_{Al}^{\alpha} = P_{Al}^{\beta} = P_{Al}^{\gamma} = 0 \qquad P_{Al}^{\delta} = 4C_{Al}$$

$$P_{A}^{\alpha} = P_{A}^{\beta} = P_{A}^{\gamma} = 1 - 4C_{Cu}\ /3 \qquad P_{A}^{\delta} = 1 - 4C_{Al}$$

    - F1b) $C_{Al} > 0.25$

$$P_{Al}^{\alpha} = P_{Al}^{\beta} = P_{Al}^{\gamma} = \left(4C_{Al} - 1\right)/3 \qquad P_{Al}^{\delta} = 1$$

$$P_{A}^{\alpha} = P_{A}^{\beta} = P_{A}^{\gamma} = 4C_{A}\ /3 \qquad P_{A}^{\delta} = 0$$

  - F2) Equally distributed in α, β, γ and δ, and:
    - F2a) $C_{Al} \leq 0.25$ and $4C_{Al} + C_A \leq 1$

$$P_{Al}^{\alpha} = P_{Al}^{\beta} = P_{Al}^{\gamma} = 0 \qquad P_{Al}^{\delta} = 4C_{Al}$$

$$P_{A}^{\alpha} = P_{A}^{\beta} = P_{A}^{\gamma} = P_{A}^{\delta} = C_A$$

    - F2b) $C_{Al} \leq 0.25$ and $4C_{Al} + C_A > 1$, or $C_{Al} > 0.25$

$$P_{Al}^{\alpha} = P_{Al}^{\beta} = P_{Al}^{\gamma} = \left(4C_{Al} - 1 + C_A\right)/3 \qquad P_{Al}^{\delta} = 1 - C_A$$

$$P_{A}^{\alpha} = P_{A}^{\beta} = P_{A}^{\gamma} = P_{A}^{\delta} = C_A$$

  - F3) Not in δ and equally distributed in α, β, γ, and:
    - F3a) $C_{Al} \leq 0.25$

$$P_{Al}^{\alpha} = P_{Al}^{\beta} = P_{Al}^{\gamma} = 0 \qquad P_{Al}^{\delta} = 4C_{Al}$$

$$P_{A}^{\alpha} = P_{A}^{\beta} = P_{A}^{\gamma} = 4C_{A}\ /3 \qquad P_{A}^{\delta} = 0$$

    - F3b) $C_{Al} > 0.25$

$$P_{Al}^{\alpha} = P_{Al}^{\beta} = P_{Al}^{\gamma} = \left(4C_{Al} - 1\right)/3 \qquad P_{Al}^{\delta} = 1$$

$$P_{A}^{\alpha} = P_{A}^{\beta} = P_{A}^{\gamma} = 4C_{A}\ /3 \qquad P_{A}^{\delta} = 0$$

- $L2_1$ order
- G) Binary alloys with:
  - Ga) $C_A \leq 0.25$

$$P_{A}^{\alpha} = P_{A}^{\beta} = 0 \qquad P_{A}^{\gamma} = 0 \qquad P_{A}^{\delta} = 4C_A$$

  - Gb) $C_A > 0.25$

$$P_{A}^{\alpha} = P_{A}^{\beta} = 0 \qquad P_{A}^{\gamma} = 3 - 4C_{Cu} \qquad P_{A}^{\delta} = 1$$

- H) Ternary alloys with the third element:
  - H1) Neither in α nor in β, and:
    - H1a) $C_{Al} \leq 0.25$

$$P_{Al}^{\alpha}=P_{Al}^{\beta}=0 \qquad P_{Al}^{\gamma}=0 \qquad P_{Al}^{\delta}=4C_{Al}$$

$$P_{A}^{\alpha}=P_{A}^{\beta}=0 \qquad P_{A}^{\gamma}=3-4C_{Cu} \qquad P_{A}^{\delta}=1-4C_{Al}$$

- H1b) $C_{Al}>0.25$

$$P_{Al}^{\alpha}=P_{Al}^{\beta}=0 \qquad P_{Al}^{\gamma}=4C_{Al}-1 \qquad P_{Al}^{\delta}=1$$

$$P_{A}^{\alpha}=P_{A}^{\beta}=0 \qquad P_{A}^{\gamma}=4C_{A} \qquad P_{A}^{\delta}=0$$

- H2) Equally distributed in α, β, γ and δ, and:

- H2a) $C_{Al}\leq 0.25$ and $4C_{Al}+C_{A}\leq 1$

$$P_{Al}^{\alpha}=P_{Al}^{\beta}=0 \qquad P_{Al}^{\gamma}=0 \qquad P_{Al}^{\delta}=4C_{Al}$$

$$P_{A}^{\alpha}=P_{A}^{\beta}=C_{A} \qquad P_{A}^{\gamma}=C_{A} \qquad P_{A}^{\delta}=C_{A}$$

- H2b) $C_{Al}\leq 0.25$ and $4C_{Al}+C_{A}>1$, or $C_{Al}>0.25$

$$P_{Al}^{\alpha}=P_{Al}^{\beta}=0 \qquad P_{Al}^{\gamma}=4C_{Al}-1+C_{A} \qquad P_{Al}^{\delta}=1-C_{A}$$

$$P_{A}^{\alpha}=P_{A}^{\beta}=C_{A} \qquad P_{A}^{\gamma}=C_{A} \qquad P_{A}^{\delta}=C_{A}$$

- H3) Neither in γ nor in δ, equally distributed in α and β, and:

- H3a) $C_{Al}\leq 0.25$

$$P_{Al}^{\alpha}=P_{Al}^{\beta}=0 \qquad P_{Al}^{\gamma}=0 \qquad P_{Al}^{\delta}=4C_{Al}$$

$$P_{A}^{\alpha}=P_{A}^{\beta}=2C_{A} \qquad P_{A}^{\gamma}=0 \qquad P_{A}^{\delta}=0$$

- H3b) $C_{Al}>0.25$

$$P_{Al}^{\alpha}=P_{Al}^{\beta}=0 \qquad P_{Al}^{\gamma}=4C_{Al}-1 \qquad P_{Al}^{\delta}=1$$

$$P_{A}^{\alpha}=P_{A}^{\beta}=2C_{A} \qquad P_{A}^{\gamma}=0 \qquad P_{A}^{\delta}=0$$